Geophysical Research Letters

RESEARCH LETTER
10.1029/2022GL100036

Analysis of Turbulence Reports and ERA5 Turbulence Diagnostics in a Tropopause-Based Vertical Framework

T. Kaluza[1], D. Kunkel[1], and P. Hoor[1]

[1]Johannes Gutenberg University Mainz, Mainz, Germany

Key Points:

- Atmospheric turbulence over the winter North Atlantic exhibits a pronounced tropopause-following behavior
- Tropopause-based mapping sorts turbulence diagnostics by atmospheric layer and reveals distinct features in the vertical distribution
- Turbulence occurs comparatively frequently in the layer which is colocated to the chemical transition between troposphere and stratosphere

Supporting Information:

Supporting Information may be found in the online version of this article.

Correspondence to:

T. Kaluza,
kaluzat@uni-mainz.de

Citation:

Kaluza, T., Kunkel, D., & Hoor, P. (2022). Analysis of turbulence reports and ERA5 turbulence diagnostics in a tropopause-based vertical framework. *Geophysical Research Letters*, *49*, e2022GL100036. https://doi.org/10.1029/2022GL100036

Received 14 JUN 2022
Accepted 3 OCT 2022

Author Contributions:

Conceptualization: T. Kaluza, D. Kunkel, P. Hoor
Formal analysis: T. Kaluza
Funding acquisition: D. Kunkel, P. Hoor
Methodology: T. Kaluza, D. Kunkel, P. Hoor
Resources: D. Kunkel, P. Hoor
Supervision: D. Kunkel, P. Hoor
Visualization: T. Kaluza
Writing – original draft: T. Kaluza
Writing – review & editing: T. Kaluza, D. Kunkel, P. Hoor

Abstract In the tropopause region turbulence exhibits a common feature with posing a threat for aviation as well as presenting a pathway for cross tropopause exchange. However, current numerical weather prediction and in particular climate models still struggle to resolve a large part of the dynamics responsible for turbulence generation. This renders high resolution observations of turbulence to be very valuable to identify the spatio-temporal distribution of turbulence. In this study we use aircraft observations along with reanalysis data over the North Atlantic during winter season to analyze turbulence occurrence. Using a tropopause-based coordinate system, we found that turbulence occurs within a sharp unimodal distribution which maximizes just below the tropopause. Turbulence also significantly affects the first 2 km above the tropopause which highlights its potential impact on the formation of the so called extratropical mixing layer around the tropopause.

Plain Language Summary Besides its importance for aviation safety atmospheric turbulence is of general interest in atmospheric sciences. It is of fundamental importance due its capability to mix air masses of different origin, fluid dynamical properties, and chemical composition. The mixing of trace gases can significantly influence the atmospheric chemistry as well as the overall radiative budget. Particularly at the tropopause, a conceptual transport barrier which separates the troposphere from the stratosphere where turbulence may play a key role to overcome this barrier. Turbulence occurs intermittently and on scales below the resolution of numerical weather prediction models. Therefore it is important to compare turbulence measurements with resolved flow characteristics in the model, to identify turbulence and diagnose its effect on the atmosphere. This study approaches this issue by comparing a comprehensive data set of turbulence measurements with a contemporary model derived representation of the atmospheric state. The analysis highlights the significance of the tropopause location to identify turbulence, diagnose the underlaying processes, and assess the viability of common turbulence diagnostics. First, our results provide insight into the degree of separation between the troposphere and the stratosphere. Second they could help to improve numerical model diagnostics to identify and forecast atmospheric turbulence.

1. Introduction

The occurrence of turbulence in the tropopause region is of general interest due to the safety hazard turbulence poses for aviation, as well as due to its impact on the distribution of atmospheric trace gases which can significantly modify the radiative budget not only locally but also at the Earth's surface (Forster & Shine, 1997). Uncertainties in the occurrence and significance of mixing processes at the tropopause on the resulting vertical distribution of trace gases like H_2O or O_3 contribute significantly to the uncertainty of their climate impact (Riese et al., 2012).

Atmospheric turbulence generally occurs on spatial scales which are not explicitly resolved in numerical weather prediction (NWP) models. Model derived turbulence diagnostics are therefore based on spatial and/or temporal gradients in gridded NWP fields which are linked to the local or developing potential for flow instabilities to occur (Sharman et al., 2006). These can ultimately result in subgrid-scale turbulence through the downward cascade of energy. Clear air turbulence as one central turbulence category is commonly associated with dynamic shear instability in stably stratified flow as the underlying mechanism (Dutton & Panofsky, 1970). According to linear theory it can occur when the nondimensional gradient Richardson number $Ri = N^2/S^2$ falls below a critical limit of $Ri_c = 1/4$ (Miles, 1961). The dimensionless ratio is composed of the static stability $N^2 = g/\Theta \cdot (\partial\Theta/\partial z)$ and the vertical shear of the horizontal wind $S^2 = (\partial u/\partial z)^2 + (\partial v/\partial z)^2$, with Earth's gravitational acceleration g, the potential temperature Θ, and the horizontal wind components u and v. Based on the Richardson number criterion,

the large scale potential for dynamic instability and turbulence is prescribed by the mean stratification and the occurrence of atmospheric wind maxima.

In the upper troposphere and lower stratosphere (UTLS) the buoyant component is dominated by the transition from mean tropospheric stratification $\overline{N^2}_{trop.} = 1 \cdot 10^{-4}\,s^{-2}$ to the stably stratified stratosphere with $\overline{N^2}_{strat.} = 4 \cdot 10^{-4}\,s^{-2}$. The transition is marked by the tropopause, which can be defined either thermally as the lapse rate tropopause, (LRT, WMO (1957)) or dynamically (Hoskins et al., 1985), and which can be regarded as a quasi-impermeable surface between the troposphere and the stratosphere. Ultimately, only the presence of nonconservative processes like for example, turbulence can foster the exchange between these two adjacent atmospheric layers. While marking a conceptual barrier on the one hand, the tropopause is on the other hand specifically affected by processes which lead to strong wind shear along with an enhanced potential for turbulent mixing. In general this is caused by the link between the large scale temperature and wind profile through the thermal wind relation (Endlich & McLean, 1965), divergent outflow of ascending air at the tropopause (Trier et al., 2020), and gravity wave induced modification of N^2 and S^2 on a large spectrum of scales (Dunkerton, 1997; Sharman et al., 2012).

The interrelation between the sharpness of the tropopause and the occurrence of strong wind shear has been analyzed for different regions and seasons (Birner, 2006; Birner et al., 2002; Sunilkumar et al., 2015; Zhang et al., 2015, 2019) and recently based on a comprehensive ECMWF (European Center for Medium-Range Weather Forecast) ERA5 atmospheric reanalysis data set (Kaluza et al., 2021). The ERA5 revealed among others a distinct occurrence frequency maximum for strong vertical wind shear at the tropopause in the North Atlantic storm track region, which peaks during winter along with the maximum meridional baroclinicity and polarfront jet stream strength.

The comparatively low tropopause altitudes during winter have the consequence that the common cruise altitudes for commercial aircraft in the North Atlantic Organized Track System are situated in the UTLS. Several commercial airlines nowadays have implemented turbulence measurements into their reporting system for meteorological data. In this context the EDR $= \epsilon^{1/3}$ as a measure for the eddy dissipation rate ϵ is becoming the aircraft-independent standard measure (Sharman et al., 2014). In this study we use these turbulence observations along with ERA5 reanalysis data to address the following question: What is the implication of the occurrence frequency maximum of enhanced wind shear above the tropopause (Kaluza et al., 2021) for the vertical distribution of dynamic instability and atmospheric turbulence? We will focus on the North Atlantic winter season UTLS, where comprehensive turbulence reports are available.

2. Data and Methods

The analysis is based on automated turbulence reports for three winter seasons (DJF) from December 2016 to February 2019 over the North Atlantic (60° W–0° W, 35° N–60° N). The turbulence reports are provided by several airlines (American, Delta, Federal Express, Northwest, United, and United Parcel Service) which downlink the data either routinely every minute or at larger time intervals with additional "triggered" reports above a certain EDR threshold (Sharman et al., 2014). The measurements used in this study are report time, geographic location, static air pressure and 1 minute peak EDR. The Meteorological Assimilation Data Ingest System applies a set of internal consistency checks to the measurements. We separate out reports where the location (altitude/latitude/longitude) of the airplane is flagged as either questioned or rejected. Spatio-temporal matching of the almost $2.1 \cdot 10^6$ remaining EDR reports with ERA5 gridded data is achieved through nearest neighbor search in the horizontal, and linear interpolation in the vertical using pressure as well as linear interpolation in time. A detailed description of the reporting technique and the quality control is given in the Supporting Information S1.

The ECMWF ERA5 reanalysis fields are analyzed on a regular 0.25° latitude-longitude grid, native vertical hybrid sigma-pressure levels, and a time resolution of 1 hour (Hersbach et al., 2020). Turbulence diagnostics and their constituents are computed as outlined in Sharman et al. (2006). The LRT altitude is determined following the definition of the WMO (1957), and as dynamic tropopause we use the uppermost level where the potential vorticity equals $Q = 2$ pvu (Hoskins et al., 1985).

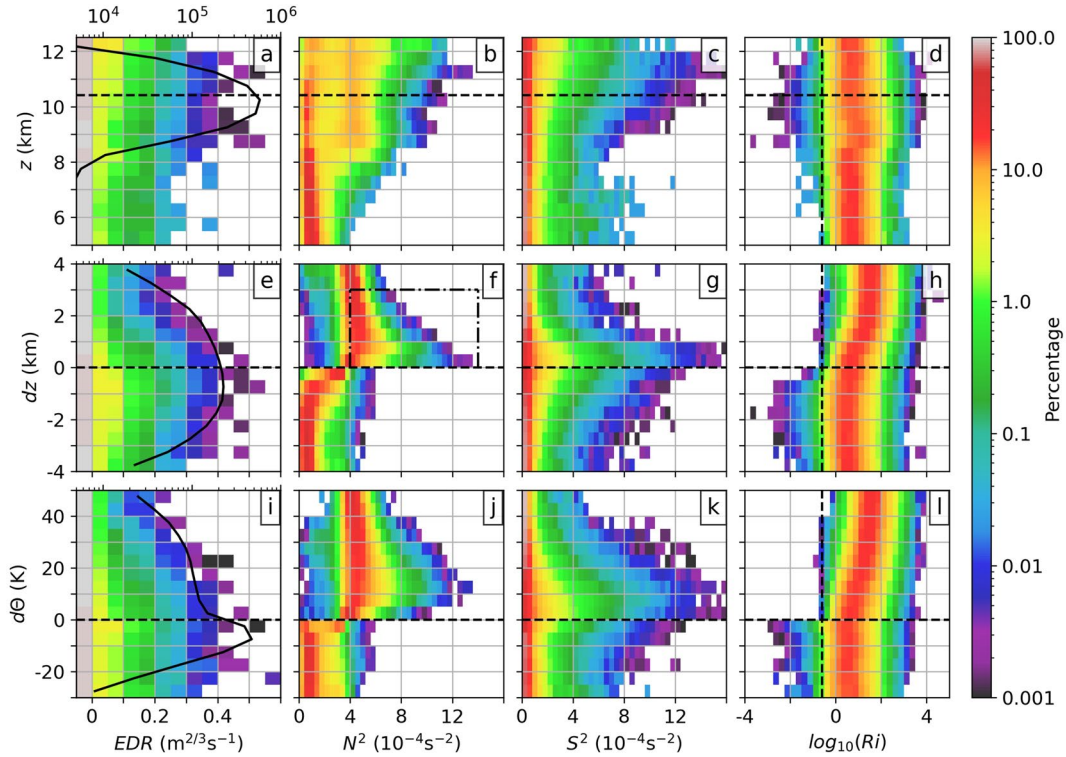

Figure 1. Vertical distribution of EDR reports and associated ERA5 turbulence diagnostics for the three analyzed DJF seasons over the North Atlantic. Relative occurrence frequencies within each altitude bin, logarithmic color scale. Top panels in a surface-based vertical framework (z, in km), middle and bottom panels in a framework based on the local distance from the lapse rate tropopause (LRT) in geometric height (dz, in km) and potential temperature ($d\Theta$, in K). Horizontal black dashed lines indicate mean LRT altitude. First column shows EDR (in $m^{2/3}s^{-1}$) as well as the vertical distribution of all turbulence reports (zero and nonzero, solid black line and upper logarithmic scale). Second column shows static stability (N^2 in s^{-2}) with the tropopause inversion layer (TIL) marked by the dash-dotted lines, third column vertical wind shear (S^2 in s^{-2}), and fourth column the logarithm of the Richardson number with the critical value $Ri_c = 1/4$ indicated by the vertical line.

This study also includes In-service Aircraft for a Global Observing System (IAGOS, Petzold et al., 2015) data. About 420 flight hours of carbon monoxide (CO) measurements from the IAGOS-CORE data set for the three winter seasons over the North Atlantic are selected and matched with ERA5 gridded data in order to assign a local tropopause altitude.

3. Turbulence Reports and Model Diagnostics in a Tropopause-Relative Framework

The vertical distribution of all turbulence reports reflects the common cruise altitudes in the North Atlantic Organized Track System (Figure 1a). The data set represents both upper tropospheric as well as lower stratospheric turbulence statistics. According to the associated relative vertical EDR distribution turbulence occurs most frequently at high altitudes in the UTLS, with maximum occurrence frequencies at highest altitudes around 12 km. The analysis of the turbulence reports based on the local vertical distance from the LRT (Figure 1e) results in a unimodal distribution which peaks at about 1 km below the LRT. The occurrence frequency maximum decreases gradually over the first 1–2 km above the LRT. In potential temperature coordinates the maximum is located within the first 5 K below the LRT (Figure 1i) and decreases over a range of 20–30 K in the stratosphere (Hoor et al., 2004), in the region of closely spaced isentropic layers associated with the tropopause inversion layer (TIL) above the LRT (Birner et al., 2002).

The 2d-histogram of static stability N^2 over the North Atlantic (Figure 1b) exhibits a unimodal distribution in the middle troposphere, with maximum occurrence frequencies at $\overline{N^2}_{trop.} = 1 \cdot 10^{-4}\ s^{-2}$. In the UTLS the distribution becomes bimodal with a second maximum at $\overline{N^2}_{strat.} = 4 \cdot 10^{-4}\ s^{-2}$, indicating the tropopause variability.

The distribution of vertical wind shear S^2 (Figure 1c) broadens with increasing altitude toward larger values, with maximum wind shear in the lower stratosphere where it can be sustained by the larger stratification. Using the LRT as a reference level takes the tropopause variability into account and reveals the TIL above the LRT (Figure 1f). Peak vertical wind shear (Figure 1g) is now strongly concentrated in a distinct layer above the LRT (Kaluza et al., 2021).

The resulting Richardson number distribution in surface-based vertical coordinates (Figure 1d) shows little variability over the depicted altitude range. In the tropopause-based framework (Figure 1h) a clear break is evident at the LRT. In the troposphere, low and subcritical Richardson numbers are evident within the logarithmic frequency range displayed. In the stratosphere this is no longer the case which indicates overall larger dynamic stability in the stratosphere, under consideration of the following two caveats. On one hand the model-based bulk Richardson numbers underrepresent the occurrence of low Richardson numbers at subgrid scales. On the other hand Schäfler et al. (2020) recently showed a systematic underestimation of vertical wind shear near the tropopause in the IFS, rendering our results to be rather conservative in the occurrence frequency with respect to shear instabilities in this region. Subcritical Richardson numbers and dynamic instabilities above the tropopause have been observed and analyzed (e.g., Kunkel et al., 2019; Trier et al., 2020; Whiteway et al., 2004). However, NWP models generally do not fully resolve the underlaying momentum and temperature gradients.

The comparatively frequent occurrence of turbulence within the first few kilometers above the LRT (Figure 1e) cannot be associated with subcritical Richardson numbers in the ERA5 (Figure 1h). Therefore we resort to the TI1 (Ellrod & Knapp, 1992), a well established turbulence diagnostic which combines vertical wind shear with the total flow deformation. The forecast skill of the flow deformation as a turbulence diagnostic has been linked to frontogenesis and thermal wind shear enhancement (Ellrod & Knapp, 1992), local gravity wave activity (e.g., Kunkel et al., 2014), and gravity wave excitation based on Lighthill-Ford theory (Knox et al., 2008). The vertical distribution of both the flow deformation (Figure 2a) as well as the TI1 (Figure 2b) exhibits little variability from 5 to 12.5 km altitude in the surface-based vertical framework. A lognormal fit over the vertically averaged TI1 distribution within this altitude range results in fit parameters $\mu_{\ln(TI1)} = -15.13$ (mean) and $\sigma_{\ln(TI1)} = 1.09$ (standard deviation). Our results are thus of the same order as those reported by Sharman and Pearson (2017) (compare their Figure 1) and Bechtold et al. (2021) ($\mu_{\ln(TI1)} = -15.4$, $\sigma_{\ln(TI1)} = 1.25$). Differences arise from the different numerical models, region, season, and altitude range. Figure 2e shows a distinct maximum for the TI1 around the LRT in the tropopause-based vertical framework, which is composed of enhanced values of the flow deformation (Figure 2d) as well as the distinct wind shear maximum (Figure 1g). This indicates that the lognormal mapping of the vertically averaged TI1 onto the climatological EDR distribution likely results in an overprediction of turbulence at the LRT.

Our study is closely related to a group of observational studies that examined mixing in the vicinity of the tropopause using tracer relationships (Fischer et al., 2000; Hoor et al., 2002; Zahn et al., 2000). In particular, using the O_3-CO relationship in the midlatitude tropopause region, Fischer et al. (2000) and Hoor et al. (2002) have concluded that a mixing layer is formed in the lowermost stratosphere right above the tropopause, as a result of troposphere to stratosphere transport. This mixing layer has later been referred to as the extratropical transition layer (ExTL) between troposphere and stratosphere (WMO, 2003). The CO measurements from the IAGOS data set are presented to illustrate the assumed link between turbulent mixing at the tropopause and the ExTL. The CO mixing ratio in the surface-based framework includes both tropospheric CO variability and tropopause variability (Figure 2c). Since the CO gradient changes at the tropopause, the tropopause-based framework accounts for the latter source of variability (Figure 2f). The distribution is now characterized by large variability in the troposphere, a transition region around the LRT with a pronounced vertical gradient along with a decreasing spread, and ultimately a vanishing vertical gradient and low spread as the mixing ratios approach stratospheric source-sink equilibrium. Enhanced CO variability as well as a pronounced vertical gradient are evident within the first 1–2 km above the LRT. The bottom panels in Figures 1 and 2 display all observational and model derived measures in an LRT-based framework with the potential temperature difference $d\Theta$ as the vertical coordinate. Focusing on the stratospheric part, this is done to show the general link between turbulence reports, model diagnostics, and trace gas distribution in Θ-space. The vertical extent of the ExTL is often analyzed in potential temperature coordinates, to link conservation properties of trace gases under adiabatic motion with the vertical distribution in the UTLS. Although the data sets (AMDAR/IAGOS) are not directly linked, they exemplify how the formation and maintenance of the ExTL is likely linked to the vertical turbulence distribution.

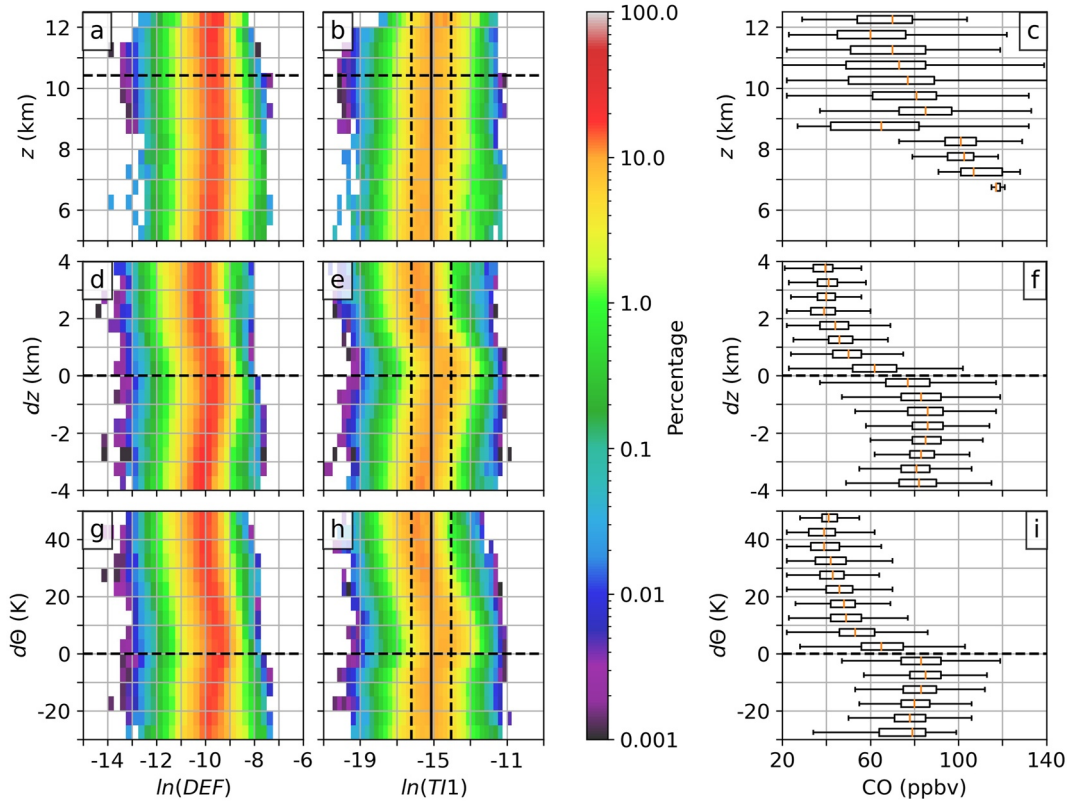

Figure 2. Continuation of Figure 1. First column shows the natural logarithm of the flow deformation calculated as in Sharman et al. (2006), and second column the TI1 index. The vertical solid and dashed black lines indicate $\mu_{\ln(TI1)}$ and $\sigma_{\ln(TI1)}$ as derived for upper flight level. The third column shows boxplots of the vertical distribution and variability of the in-service aircraft for a global observing system (IAGOS) carbon monoxide measurements for the same region and seasons as the turbulence reports.

4. ERA5 Turbulence Diagnostics at EDR Report Locations

Section 3 summarized fundamental differences in the background distribution of a set of turbulence diagnostics between the troposphere and the stratosphere. This motivates to validate these diagnostics at EDR report locations individually for both atmospheric layers. The number of nonzero turbulence reports decreases exponentially with increasing EDR (Figures 3a and 3d), which should be taken into account in the discussion of the statistical significance of the top end EDR values.

In the troposphere, turbulence occurs within a wide range of static stability according to the ERA5 (Figure 3d). At comparatively low EDR around 0.1 $m^{2/3}s^{-1}$ the N^2 distribution broadens at the lower end, indicating a tendency toward convective instability (actual convective instability, if resolved, is neglected due to the logarithmic scale). With increasing EDR the N^2 distribution converges at larger values, as does the vertical wind shear (Figure 3e). This could indicate an increased relevance of shear instability in stably stratified flow for stronger turbulence. The associated Richardson numbers rarely fall below the critical threshold (Figure 3f), however, previous studies have shown that the IFS is only capable to resolve bulk Richardson numbers of the order of 1 for observed dynamic instability in the UTLS (e.g., Kunkel et al., 2019). A systematic underestimation of strong vertical wind shear in the IFS should also be considered, particularly in the tropopause region (Schäfler et al., 2020) where strong turbulence is most common (Figure 1e). Still, other processes like the dissipation of non-resolved gravity waves or local convective instability cannot be ruled out as additional sources for the encountered turbulence.

In the stratosphere the Richardson number distribution is shifted toward even larger values (Figure 3c). It peaks at about $Ri = 1$ with a negligible percentage of subcritical Richardson numbers, in agreement with the results discussed in Section 3. The static stability exhibits a narrow distribution (Figure 3a) which peaks at the stratospheric background of $N^2 = 4 \cdot 10^{-4}\ s^{-2}$. The vertical wind shear shows enhanced values over the whole range

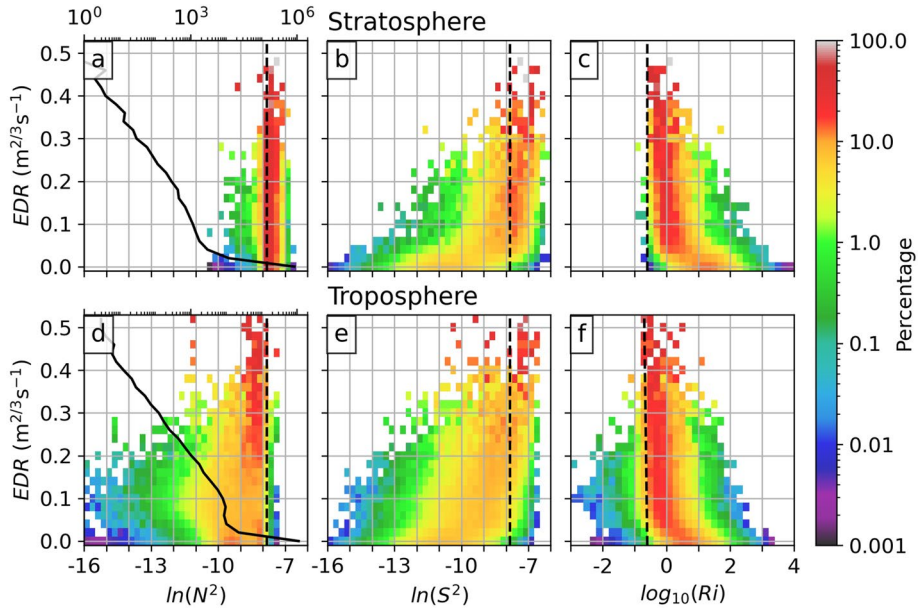

Figure 3. Spatio-temporal matching of turbulence diagnostics from ERA5 at EDR report locations. Relative occurrence frequency normalized within each EDR bin, in logarithmic color scale. Bottom panels show tropospheric (below the LRT) and top panels stratospheric (above the LRT) turbulence reports. Panels (a) and (d) show static stability N^2 (in s^{-2}) and the distribution of measured EDR (absolute count, solid black line and exponential top scale). Panels (b) and (e) show vertical wind shear S^2 (in s^{-2}), and panels (c) and (f) the logarithm of the Richardson number. Vertical dashed lines indicate $N^2 = 4 \cdot 10^{-4}$ s^{-2}, $S^2 = 4 \cdot 10^{-4}$ s^{-2} and $Ri_c = 1/4$.

of nonzero EDR bins (Figure 3b), compared to the nonturbulent background which is indicated by the lowest EDR bin. However, using wind shear alone as a quantitative diagnostic for turbulence is limited, since the S^2 distribution does not change significantly for EDR $\geq 0.05\,m^{2/3}s^{-1}$. Nevertheless, we expect that the wind shear is underestimated in this region due to the limited vertical resolution as well as to the missing representation of (dissipating) gravity waves. Thus, we expect that dynamic instability is a major contributor for turbulence generation in the lower stratosphere. Additionally, the flow deformation shows enhanced values at turbulent events in both troposphere and stratosphere (see Figures 4a and 4d and following the analysis in Section 3). This has consequences for the TI1 distribution (Figures 4b and 4e). For nonzero EDR the TI1 reaches enhanced values and thus indicates the presence of turbulence. The correlation between EDR and TI1 is more pronounced compared to the ones with vertical wind shear or flow deformation. However, the distribution within each EDR bin remains wide compared to the slope, indicating the limitations in using the TI1 from ERA5 as a turbulence intensity diagnostic.

The previous analysis showed that strong vertical wind shear directly above the LRT contributes significantly to the comparatively frequent occurrence of turbulence in the stably stratified lower stratosphere. Kaluza et al. (2021) linked the occurrence of the tropopause wind shear layer over the North Atlantic with above-average potential temperatures $\Theta(Q = 2\,\text{pvu})$ at the dynamic tropopause, and thus, with ridges of Rossby waves reaching far to the north. The turbulence reports for the three analyzed winter seasons indicate that turbulence in the UTLS is in a similar way linked to the location of the dynamic tropopause. The occurrence frequency for turbulence directly above the LRT increases with $\Theta(Q = 2\,\text{pvu})$ (Figure 4c), where for example, turbulence within the whole measured EDR range is about an order of magnitude more common in regions with $\Theta(Q = 2\,\text{pvu}) = 330$ K compared to $\Theta(Q = 2\,\text{pvu}) = 300$ K. A similar but more gradual increase is evident for turbulence within the first 2 km below the LRT (Figure 4f). So in summary, while Figure 1e identified turbulence in the UTLS to be primarily a tropopause-bound feature, the analysis in this paragraph further specified that it is particularly associated with elevated tropopauses.

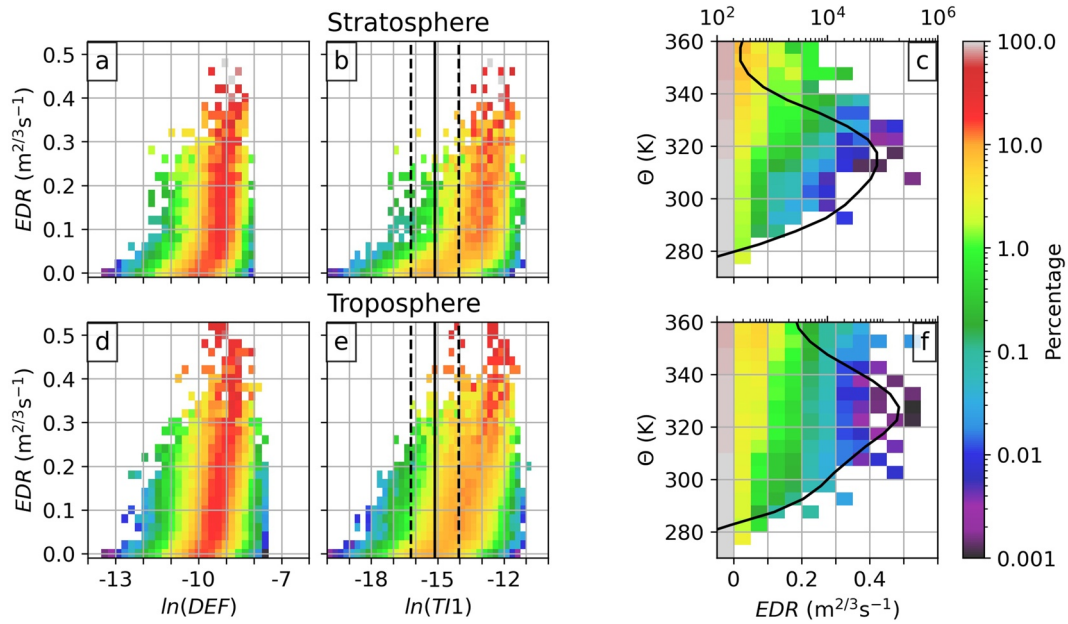

Figure 4. Continuation of Figure 3. Panels (a) and (d) show the natural logarithm of the total flow deformation. Panel (b) and (e) show the TI1 index. The vertical solid and dashed black lines indicate $\mu_{\ln(TI1)}$ and $\sigma_{\ln(TI1)}$ as derived in Section 3. Panel (c) shows the measured EDR occurrence frequency distribution within the first 1 km above the LRT depending on the potential temperature $\Theta(Q = 2\,\text{pvu})$ at the local dynamic tropopause. Note the increasing occurrence frequency with increasing $\Theta(Q = 2\,\text{pvu})$. The associated turbulence report count with respect to $\Theta(Q = 2\,\text{pvu})$ is indicated by the solid black line and the logarithmic upper x-scale. Panel (f) shows the equivalent analysis for the first 2 km below the LRT. The colorbar is representative for all six panels.

5. Summary and Discussion

This study highlights the importance of the tropopause location for the occurrence of turbulence, based on the analysis of turbulence reports and associated model derived turbulence diagnostics. The analysis of the turbulence reports in a tropopause-based vertical framework reveals a unimodal occurrence frequency distribution, which peaks about one km below the LRT, and decreases gradually in the lower stratosphere within a layer that follows the tropopause.

On the basis of chemical composition gradients this region has been defined as the ExTL, which exhibits both stratospheric as well as tropospheric characteristics due to stratosphere-troposphere exchange and mixing processes. The associated separation of a mixed layer from the stratosphere above has been attributed to a distinct change in transport timescales (Berthet et al., 2007; Hoor et al., 2010). The present study highlights the importance of turbulence occurrence as a highly transient, but frequent mixing process at the extratropical tropopause. As such it may play a crucial role for the formation and maintenance of the ExTL (Konopka & Pan, 2012), aside from other processes like convective injection (Homeyer et al., 2014) or radiatively induced PV modification along with STE (Zierl & Wirth, 1997).

Furthermore, the analysis provides insight into the vertical distribution of turbulence and the underlying atmospheric flow features at flight levels between 5 and 12.5 km altitude. It indicates a significant contribution of strong vertical wind shear at the tropopause for the generation of stratospheric turbulence over the winter North Atlantic storm track region. In this area the wind shear is closely linked to the baroclinic wave activity along with the associated tropopause variability (Kaluza et al., 2021). Further research should address the question of seasonal and geographical differences in the turbulence occurrence in a tropopause-relative framework, as well as its variability over a vertical range that is not limited to commercial airline cruise altitudes.

The separate analysis of tropospheric and stratospheric turbulence encounters indicates the varying importance of convective and dynamic instability as turbulence generating processes, and provides further insight into the deficit of numerical models to resolve these processes. It furthermore reveals structures in the tropopause-relative

vertical distribution of the model derived turbulence diagnostics which are not evident in the surface based framework. This could help to improve common state-of-the-art approaches to identify, diagnose and forecast turbulence in numerical models (Bechtold et al., 2021; Muñoz-Esparza et al., 2020; Sharman & Pearson, 2017).

Data Availability Statement

Aircraft base observations from the public NOAA archive are available upon request at https://madis.ncep.noaa.gov (last accessed 27 July 2022). ECMWF's ERA5 data can be freely accessed from https://www.ecmwf.int/en/forecasts/datasets/reanalysis-datasets/era5 (Hersbach et al., 2020). The up-to-date In-service aircraft for a global observing system data are publicly available at http://www.iagos.fr thanks to support from AERIS (last accessed 27 July 2022).

Acknowledgments
This study was made possible in part due to the data made available to the National Oceanic and Atmospheric Administration by the following commercial airlines: American, Delta, Federal Express, Northwest, United, and United Parcel Service. We thank the ECMWF for freely providing ERA5 data which has been retrieved from the MARS system. In-service aircraft for a global observing system (IAGOS) data were created with support from the European Commission, national agencies in Germany (BMBF), France (MESR), and the UK (NERC), and the IAGOS member institutions (http://www.iagos.org/partners). The participating airlines (Lufthansa, Air France, Austrian, China Airlines, Iberia, Cathay Pacific, Air Namibia, Sabena) supported IAGOS by carrying the measurement equipment free of charge since 1994. This study is funded by the Deutsche Forschungsgemeinschaft (DFG, German Research Foundation) – TRR 301 – Project-ID 428312742. It is furthermore supported by the project "Big Data in Atmospheric Physics (BINARY)," funded by the Carl Zeiss Foundation (Grant P2018-02-003). We acknowledge the ZDV of the Johannes Gutenberg University and the Mogon II Super Cluster for providing the necessary hardware to analyze the data. Special thanks to R. Sharman and M. Bramberger for an encouraging discussion and for providing insight into details of the GTG and the turbulence reports. Open access funding enabled and organized by Projekt DEAL.

References

Bechtold, P., Bramberger, M., Dörnbrack, A., Leutbecher, M., Isaksen, L., Memo, T., et al. (2021). Experimenting with a clear air turbulence (CAT) index from the IFS (tech. Rep.). https://doi.org/10.21957/4l34tqljm

Berthet, G., Esler, J. G., & Haynes, P. H. (2007). A Lagrangian perspective of the tropopause and the ventilation of the lowermost stratosphere. *Journal of Geophysical Research*, *112*(18), 1–14. https://doi.org/10.1029/2006JD008295

Birner, T. (2006). Fine-scale structure of the extratropical tropopause region. *Journal of Geophysical Research*, *111*(4), 1–14. https://doi.org/10.1029/2005JD006301

Birner, T., Dörnbrack, A., & Schumann, U. (2002). How sharp is the tropopause at midlatitudes? *Geophysical Research Letters*, *29*(14), 45–1–45–4. https://doi.org/10.1029/2002GL015142

Dunkerton, T. J. (1997). Shear instability of internal inertia-gravity waves. *Journal of the Atmospheric Sciences*, *54*(12), 1628–1641. https://doi.org/10.1175/1520-0469(1997)054<1628:SIOIIG>2.0.CO;2

Dutton, J. A., & Panofsky, H. A. (1970). Clear air turbulence: A mystery may be unfolding. *Science*, *167*(3920), 937–944. https://doi.org/10.1126/science.167.3920.937

Ellrod, G. P., & Knapp, D. I. (1992). An objective clear-air turbulence forecasting technique: Verification and operational use. *Weather and Forecasting*, *7*(1), 150–165. https://doi.org/10.1175/1520-0434(1992)007<0150:AOCATF>2.0.CO;2

Endlich, R. M., & McLean, G. S. (1965). Jet-stream structure over the central United States determined from aircraft observations. *Journal of Applied Meteorology*, *4*(1), 83–90. https://doi.org/10.1175/1520-0450(1965)004<0083:JSSOTC>2.0.CO;2

Fischer, H., Wienhold, F. G., Hoor, P., Bujok, O., Schiller, C., Siegmund, P., et al. (2000). Tracer correlations in the northern high latitude lowermost stratosphere: Influence of cross-tropopause mass exchange. *Geophysical Research Letters*, *27*(1), 97–100. https://doi.org/10.1029/1999GL010879

Forster, P. M. D. E., & Shine, K. P. (1997). Radiative forcing and temperature trends from stratospheric ozone changes. *Journal of Geophysical Research*, *102*(D9), 10841–10855. https://doi.org/10.1029/96JD03510

Hersbach, H., Bell, B., Berrisford, P., Hirahara, S., Horányi, A., Muñoz-Sabater, J., et al. (2020). The ERA5 global reanalysis. *Quarterly Journal of the Royal Meteorological Society*, *146*(730), 1–51. https://doi.org/10.1002/qj.3803

Homeyer, C. R., Pan, L. L., Dorsi, S. W., Avallone, L. M., Weinheimer, A. J., O'Brien, A. S., et al. (2014). Convective transport of water vapor into the lower stratosphere observed during double-tropopause events. *Journal of Geophysical Research*, *119*(18), 10941–10958. https://doi.org/10.1002/2014JD021485

Hoor, P., Fischer, H., Lange, L., Lelieveld, J., & Brunner, D. (2002). Seasonal variations of a mixing layer in the lowermost stratosphere as identified by the CO-O_3 correlation from in situ measurements. *Journal of Geophysical Research*, *107*(D5), ACL1–1–ACL1–11. https://doi.org/10.1029/2000JD000289

Hoor, P., Gurk, C., Brunner, D., Hegglin, M. I., Wernli, H., & Fischer, H. (2004). Seasonality and extent of extratropical TST derived from in-situ CO measurements during SPURT. *Atmospheric Chemistry and Physics Discussions*, *4*(2), 1691–1726. https://doi.org/10.5194/acp-4-1427-2004

Hoor, P., Wernli, H., Hegglin, M. I., & Bönisch, H. (2010). Transport timescales and tracer properties in the extratropical UTLS. *Atmospheric Chemistry and Physics*, *10*(16), 7929–7944. https://doi.org/10.5194/acp-10-7929-2010

Hoskins, B. J., McIntyre, M. E., & Robertson, A. W. (1985). On the use and significance of isentropic potential vorticity maps. *The Quarterly Journal of the Royal Meteorological Society*, *111*(466), 877–946. https://doi.org/10.1002/qj.49711147002

Kaluza, T., Kunkel, D., & Hoor, P. (2021). On the occurrence of strong vertical wind shear in the tropopause region: A 10-year ERA5 northern hemispheric study. *Weather and Climate Dynamics*, *2*(3), 631–651. https://doi.org/10.5194/wcd-2-631-2021

Knox, J. A., McCann, D. W., & Williams, P. D. (2008). Application of the Lighthill-Ford theory of spontaneous imbalance to clear-air turbulence forecasting. *Journal of the Atmospheric Sciences*, *65*(10), 3292–3304. https://doi.org/10.1175/2008JAS2477.1

Konopka, P., & Pan, L. L. (2012). On the mixing-driven formation of the extratropical transition layer (ExTL). *Journal of Geophysical Research*, *117*(17), 1–9. https://doi.org/10.1029/2012JD017876

Kunkel, D., Hoor, P., Kaluza, T., Ungermann, J., Kluschat, B., Giez, A., et al. (2019). Evidence of small-scale quasi-isentropic mixing in ridges of extratropical baroclinic waves. *Atmospheric Chemistry and Physics*, *19*(19), 12607–12630. https://doi.org/10.5194/acp-19-12607-2019

Kunkel, D., Hoor, P., & Wirth, V. (2014). Can inertia-gravity waves persistently alter the tropopause inversion layer? *Geophysical Research Letters*, *41*(22), 7822–7829. https://doi.org/10.1002/2014GL061970

Miles, J. W. (1961). On the stability of heterogeneous shear flows. *Journal of Fluid Mechanics*, *10*(4), 496–508. https://doi.org/10.1017/S0022112061000305

Muñoz-Esparza, D., Sharman, R. D., & Deierling, W. (2020). Aviation turbulence forecasting at upper levels with machine learning techniques based on regression trees. *Journal of Applied Meteorology and Climatology*, *59*(11), 1883–1899. https://doi.org/10.1175/JAMC-D-20-0116.1

Petzold, A., Thouret, V., Gerbig, C., Zahn, A., Brenninkmeijer, C. A., Gallagher, M., et al. (2015). Global-scale atmosphere monitoring by in-service aircraft - Current achievements and future prospects of the European research infrastructure iagos. *Tellus Series B Chemical and Physical Meteorology*, *6*, 1–24. https://doi.org/10.3402/tellusb.v67.28452

Riese, M., Ploeger, F., Rap, A., Vogel, B., Konopka, P., Dameris, M., & Forster, P. (2012). Impact of uncertainties in atmospheric mixing on simulated UTLS composition and related radiative effects. *Journal of Geophysical Research*, *117*(16), 1–10. https://doi.org/10.1029/2012JD017751

Schäfler, A., Harvey, B., Methven, J., Doyle, J. D., Rahm, S., Reitebuch, O., et al. (2020). Observation of jet stream winds during nawdex and characterization of systematic meteorological analysis errors. *Monthly Weather Review*, *148*(7), 2889–2907. https://doi.org/10.1175/MWR-D-19-0229.1

Sharman, R. D., Cornman, L. B., Meymaris, G., Pearson, J., & Farrar, T. (2014). Description and derived climatologies of automated in situ eddy-dissipation-rate reports of atmospheric turbulence. *Journal of Applied Meteorology and Climatology*, *53*(6), 1416–1432. https://doi.org/10.1175/JAMC-D-13-0329.1

Sharman, R. D., & Pearson, J. M. (2017). Prediction of energy dissipation rates for aviation turbulence. Part I: Forecasting nonconvective turbulence. *Journal of Applied Meteorology and Climatology*, *56*(2), 317–337. https://doi.org/10.1175/JAMC-D-16-0205.1

Sharman, R. D., Tebaldi, C., Wiener, G., & Wolff, J. (2006). An integrated approach to mid- and upper-level turbulence forecasting. *Weather and Forecasting*, *21*(3), 268–287. https://doi.org/10.1175/WAF924.1

Sharman, R. D., Trier, S. B., Lane, T. P., & Doyle, J. D. (2012). Sources and dynamics of turbulence in the upper troposphere and lower stratosphere: A review. *Geophysical Research Letters*, *39*(12). https://doi.org/10.1029/2012GL051996

Sunilkumar, S. V., Muhsin, M., Parameswaran, K., Venkat Ratnam, M., Ramkumar, G., Rajeev, K., et al. (2015). Characteristics of turbulence in the troposphere and lower stratosphere over the Indian Peninsula. *Journal of Atmospheric and Solar-Terrestrial Physics*, *133*, 36–53. https://doi.org/10.1016/j.jastp.2015.07.015

Trier, S. B., Sharman, R. D., MuñOz-Esparza, D., & Lane, T. P. (2020). Environment and mechanisms of severe turbulence in a midlatitude cyclone. *Journal of the Atmospheric Sciences*, *77*(11), 3869–3889. https://doi.org/10.1175/JAS-D-20-0095.1

Whiteway, J. A., Klaassen, G. P., Bradshaw, N. G., & Hacker, J. (2004). Transition to turbulence in shear above the tropopause. *Geophysical Research Letters*, *31*(2), 2–5. https://doi.org/10.1029/2003GL018509

WMO. (1957). Meteorology – A threedimensional science: Second session of the commission for aerology. *World Meteorological Organization Bulletin*, *VI*(4), 134–138.

WMO. (2003). Scientific assessment of ozone depletion: 2002, global ozone research and monitoring project report no. 47.

Zahn, A., Brenninkmeijer, C. A., Maiss, M., Scharffe, D. H., Crutzen, P. J., Hermann, M., et al. (2000). Identification of extratropical two-way troposphere-stratosphere mixing based on caribic measurements of O3, CO, and ultrafine particles. *Journal of Geophysical Research*, *105*(D1), 1527–1535. https://doi.org/10.1029/1999JD900759

Zhang, Y., Zhang, S., Huang, C., Huang, K., & Gong, Y. (2019). The tropopause inversion layer interaction with the inertial gravity wave activities and its latitudinal variability. *Journal of Geophysical Research: Atmospheres*, *124*(14), 7512–7522. https://doi.org/10.1029/2019JD030309

Zhang, Y., Zhang, S., Huang, C., Huang, K., Gong, Y., & Gan, Q. (2015). The interaction between the tropopause inversion layer and the inertial gravity wave activities revealed by radiosonde observations at a midlatitude station Yehui. *Journal of Geophysical Research: Atmospheres*, *175*(4449), 238–8111. https://doi.org/10.1002/2015JD023115

Zierl, B., & Wirth, V. (1997). The influence of radiation on tro-popause behavior and stratosphere-troposphere exchange in an upper tropospheric anticyclone. *Journal of Geophysical Research*, *102*(D20), 23883–23894. https://doi.org/10.1029/97JD01667